CrossMark

RESEARCH PAPER

Characterization of a miniaturized liquid bridge for nL sample infusion: a comparative study of sample flush-out behavior using flow simulations and direct ESI-MS analysis

Volker Neu[1,4] · Pablo Dörig[2,5] · Christof Fattinger[3] · Stephan Müller[3] · Renato Zenobi[1]

Abstract In this work we shed light on the microfluidics of a miniaturized liquid bridge that forms the central part of a so-called "capillary gap sampler," a novel device for rapid and seamless injection of nanoliter sample volumes into an electrospray ionization mass spectrometer (ESI-MS). Parameters relevant for sample flush-out at the liquid bridge and in the spray capillary were identified by systematic variation of the capillary dimensions, the linear buffer flow rate (2.1–34 mm/s) and molecular weight of the analytes (0.5–30 kDa). We found that a reduction in capillary wall thickness by a factor of 1.6 significantly influences analyte peak shapes, leads to an inversion of the relationship between peak width and analyte molecular weight, and allows a fivefold decrease in peak width for large molecules down to 5 s. The results could be verified and explained by simulations, in which the presence of diffusion-controlled "dead zones" at the liquid bridge and dispersion in the spray tip that depend on analyte molecular weight were identified as key factors relevant for the sample flush-out process. The merging of simulations and experimental data gives useful hints toward the re-design of a spray tip as built-in ESI-MS interface for an optimized gap sampler performance.

Keywords Capillary gap sampler · Flow injection analysis · Molecule dispersion · Peak profiles

✉ Renato Zenobi
  zenobi@org.chem.ethz.ch

1 Department of Chemistry and Applied Biosciences, ETH Zurich, 8093 Zurich, Switzerland

2 Laboratory of Biosensors and Bioelectronics, Institute of Biomedical Engineering, ETH Zurich, 8092 Zurich, Switzerland

3 F. Hoffmann-La Roche AG, pRED, Pharma Research & Early Development, Discovery Technologies, Grenzacherstrasse 124, 4070 Basel, Switzerland

4 Present Address: Competence Center Analytics, BASF SE, Carl-Bosch-Straße 38, 67056 Ludwigshafen, Germany

5 Present Address: Cytosurge AG, 8152 Glattbrugg, Switzerland

1 Introduction

Small volume liquid sampling is crucial for microfluidic systems. Moreover, direct coupling of microfluidics to comprehensive analysis techniques such as electrospray ionization mass spectrometry (ESI-MS) is an emerging field in biomedical research. The interest for merging this triad of techniques is based on the fact that biological samples are often available only in very small amounts, but show a high complexity (Gao et al. 2013). Additionally, for many applications, the speed of analysis is of central importance, e.g., in modern drug discovery, where large compound libraries need to be screened (Mayr and Bojanic 2009) or in systems biology, where different cells or subsets of functional cell components need to be screened and compared (Feng et al. 2008).

A critical point for miniaturized systems concerns the sampling of small volumes, typically in the nL-range. In this context, many types of microvalves have been developed in order to fulfill two main requirements: (1) robust and reliable sample uptake without influencing the sample composition, and (2) seamless transfer to another

miniaturized system for further sample manipulation and/or analysis (Oh and Ahn 2006).

In the following, we first describe three state-of-the-art techniques of small volume sampling in the context of coupling microfluidics to mass spectrometry: classical mechanical valves, chip-based systems, and non-chip-based systems. We then present a description of the capillary gap sampler. This is followed by a combined experimental and theoretical study aimed at describing, understanding, and better controlling the microfluidic behavior of the gap sampler.

1.1 Mechanical valve systems

In mechanical valves used for nanoliter sample injection, the traditional sample loop is replaced by an internal rotor bore. Due to the manufacturing process and assembly of compartments, mechanical valves have limitations with respect to sample volume (a few nL are the minimum), compactness (the small sample is exposed to a relatively large surface area in the sampling system), and the presence of dead zones, e.g., at connection points to solvent lines. This is especially critical for seamless valve integration into lab-on-a-chip (LOC) platforms and micro total analysis systems (µTAS). Nevertheless, mechanical valves provide high robustness and reproducibility, which makes them the devices of choice for the performance of routine flow injection analysis (Růžička 1992) also in high-throughput applications (Jian et al. 2011).

1.2 Chip-based systems

Chip-based systems for miniaturized sample analysis by mass spectrometry have been studied extensively within the last two decades (Koster and Verpoorte 2007; Ohla and Belder 2012; Feng et al. 2014). This is due to the development of micromachining processes such as photolithography, etching, hot embossing, and laser ablation, which, in combination with chip bonding, allow for the creation of very fine and compact structures (Nge et al. 2013). Chip-based microvalves suitable for on/off switching have been developed in an integrated format, e.g., by the use of in-line channels and membranes embedded into multiple layers of polymeric chip material, respectively (Oh and Ahn 2006), or a modular format, by using the microchip as part of a multicomponent assembly. In the latter case, the chip is sandwiched between the rotor and the stator of a classic mechanical valve (Yin et al. 2005). Moreover, in commercialized systems, selected chip channels are filled with an adsorptive material. This facilitates on-chip sample extraction as well as analyte concentration and separation (Yin et al. 2005; Gerhardt 2011), but also lowers the sample throughput of the system. A major drawback of

mechanical valves and chip-based systems is that lines are needed for sample introduction, which bears the risk of unspecific sample adsorption. Additionally, direct uptake and introduction of a few nL in sample volume is still challenging. Attempts to minimize sample adsorption in chip-based systems include the use of chemically inert materials such as polymer lines made of Teflon, in combination with inert system liquids such as oils and surfactants. Inert system liquids or air plugs are also used for the generation of small sample volumes in droplet-based microfluidics coupled to ESI-MS (Pei et al. 2010; Sun et al. 2012). Interesting alternatives work with electrostatic ionization of droplets directly on the chip by using a spyhole, and with IR-beam supported ionization (Volný et al. 2014; Gasilova et al. 2014).
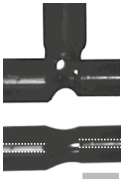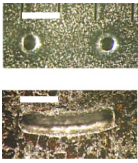
1.3 Non-chip-based systems

Non-chip-based systems for a pressure-assisted uptake of small sample volumes often work with capillaries or tips. Here, so-called liquid microjunction surface sampling (LMJ-SSP) is a widely used principle where the sample is directly extracted from a surface. Depending on the setup, sample extraction can be performed from selected spots or by continuous scanning of a surface (Van Berkel et al. 2009; Roach et al. 2010). Alternatively, laser ablation from a surface in combination with liquid extraction of the sample plume has been shown, in order to reach a higher spatial resolution in sampling (Ovchinnikova et al. 2011; Park and Murray 2012; O'Brien et al. 2015). Van Berkel's group recently presented an open port sampling interface (OPSI) which combines different sampling modes such as sampling from a plume after laser ablation, SMJ-SSP, and continuous spilling for very concentrated samples (Van Berkel and Kertesz 2015). Nevertheless, sample volumes handled within these systems are in the range of 100 nL to few microliters, based on the dimensions of the sampling device and the difficulty of an active and precise control of liquids in the nanoliter range. Another interesting sampling device called Swan probe was recently presented by Jin et al. (2014). The Swan probe can be used for sampling of few to several nL from a microfluidic droplet array or a multiwell plate, whereas the sampling volume and rate is influenced by the buffer flow rate through the probe and the contact time of probe to the sample.

1.4 Capillary gap sampler

We recently introduced a sampling platform called capillary gap sampler (Neu et al. 2013), which allows for direct and fast uptake of a few nL sample volume, combined to a line-free sample introduction into a miniaturized liquid bridge as new microfluidic element for flow injection analysis. The

Table 1 Configurations of nanoliter infusion systems used in this work

	Standard configuration	Large ID configuration	Nano-injection valve	
Images				Stator bores
				Rotor bore
Schematic (idealized)				Stator Rotor
Dimensions OD × ID (µm)	FS-line: 360 × 50 SS-tip: 320 × 50	FS-line: 360 × 220 SS-tip: 390 × 220	FS-lines: 360 × 50 Stator bores: 100	
Internal system volumes (nL)	Capillary gap: ~20 SS tip: 98	Capillary gap: ~20 SS tip: 1901	Rotor bore: ~10 FS-line to ESI nozzle: 387	

Shown are snapshots of two configurations of the liquid bridge during sample infusion using a capillary gap sampler ("standard configuration" and "large ID configuration"), as well as pictures of the rotor and stator of a commercial nano-injection valve. Dashed lines in white mark the capillary ID; white and gray bars mark a distance of 1/10″ (254 µm), respectively. Moreover, schematics and relevant parameters are given for each device; The feed reaches the gap via a fused silica (FS) capillary and leaves it toward the mass spectrometer via a stainless steel (SS) capillary

concept of the sampler is depicted in Fig S1, derived from (Neu et al. 2013). The liquid bridge is formed in the gap between two capillaries, one of which directly acts as the interface to ESI-MS. Initial system characterization showed that the stability of the liquid bridge is strongly dependent on the distance between the capillaries. Investigations of other system parameters that influence the sample flush-out behavior of the liquid bridge and the analytical performance of the sampling system have not been carried out so far.

The present work aims at identifying and understanding relevant microfluidic processes when using a liquid bridge for nL flow injection analysis. On the experimental side, this includes systematic variation of the capillary configuration, buffer flow rate, and sample composition. All these parameters influence the observed peak profiles of analytes. Obviously, direct read-out of biochemical assays in high-throughput is an application field of the sampler. In this context, analytes in a mass range of 0.5–30 kDa as well as analyte concentrations in the micromolar range have been chosen. Subsequent finite element flow simulations of the experimental data are designed to provide a better understanding of the microfluidic processes that take place in the liquid bridge and within the spray capillary. The insights obtained can then be applied for the development of an optimized spray needle design with respect to the analytical performance of the sampler.

The injection principle of the sampler of using an open liquid bridge which is not contacted directly to sample surfaces is unique. Nevertheless, studies on the influence of the geometry of the injection zone on peak profiles including variation of the buffer flow rate and analyte molecular

weight could also be relevant for the design of similar systems for miniaturized sample analysis like the swan probe (Jin et al. 2014) or sample transfer into an open solvent stream after laser ablation (Park and Murray 2012).

2 Materials and methods

2.1 Components for nanoliter injection

If not specified otherwise, the components and the setup of a capillary gap sampler are as described in a previous publication (Neu et al. 2013). In this section, only the components of the system that are in direct contact to the sample are described in detail. For creating different capillary configurations, fused silica capillaries (360 µm O.D., 50 µm I.D., Polymicro, Phoenix, AZ, USA; 360 µm O.D., 220 µm I.D., SGE, Melbourne, Australia) and stainless needles (320 µm O.D., 50 µm I.D., 50 mm length, New Objective, Woburn, MA; 390 µm O.D, 220 µm I.D., 50 mm length, Unimed, Lausanne, Switzerland) were used. For sample uptake and delivery out of a standard 384-microwell plate, a metal pin (356 µm in diameter, V&P Scientific, San Diego, CA) was used. For standardized sample infusion, a nano-injection valve (Cheminert, C4N-4004-.01PFC, VICI, Houston, TX, USA) was connected to a fused silica buffer line (360 µm O.D., 50 µm I.D., Polymicro), and to a tapered, metal coated fused silica line of 19.7 cm in length (Taper Tip, 320 µm O.D., 50 µm I.D., New Objective), which was acting as ESI interface. Sample introduction was performed by using a

1-µL syringe (#7107, Hamilton, Bonaduz, Switzerland) equipped with a syringe fill port (VISF.5FPK, VICI). Valve switching was performed manually.

2.2 Flow rate limitations

For both the standard and the large ID capillary configuration (see Table 1), flow rates <0.5 and 4.9 µL/min, respectively, lead to extremely broad peaks and very long sample residence times within the spray tip (see also Fig. 1). High residence times and broad peaks are not useful in the context of applying the sampler for fast sequential sample analysis and hence were avoided. For the standard configuration, flow rates >4 µL/min gave backpressures caused by the spray tip which exceeded the system tolerance in backpressure compensation (~200 mbar max.). For the large ID configuration, volumetric flow rates >38.8 µL/min are hardly applicable based on the design of the electrospray interface, which does not comprise heat or supporting spray gases. The distinct differences in applied volumetric flow rates between the two capillary ID configurations are applied to assure comparable linear flow velocities of both capillary configurations.

2.3 Samples and system buffer

Two analyte mixtures each consisting of leucine-enkephalin (Leu-Enk, Bachem, Bubdendorf, Switzerland), insulin β-chain disulfate (bovine, Serva, Heidelberg, Germany), myoglobin (equine heart, ≥90 % essentially salt free, Sigma-Aldrich, Buchs, Switzerland), and carbonic anhydrase II (bovine erythrocytes, Fluka) were prepared in purified water (MilliQ, Millipore, Barnstead, NH, USA) according to Table 2. System buffer was prepared by mixing purified water and methanol (LiChrosolv, Merck, Darmstadt, Germany) 50:50 (v/v), and by adding 0.1 % formic acid (eluent additive for LC-MS, Fluka).

2.4 Equipment for detection, buffer delivery, and software

Mass spectrometric detection was performed by direct coupling of the capillary gap sampler or the nano-injection valve, respectively, to a Q-ToF Ultima, (Micromass, Manchester, UK), controlled by the MassLynx software (v4.1). Buffer delivery was performed via a syringe pump (neMESYS, cetoni, Korbussen, Germany).

2.5 Numerical simulations

The flow and concentration profile simulations were performed with COMSOL Multiphysics version 4.4 (Burlington, MA, USA). The simulations assumed laminar flow and the analytes were modeled, in a 2D rotational symmetric case, with the
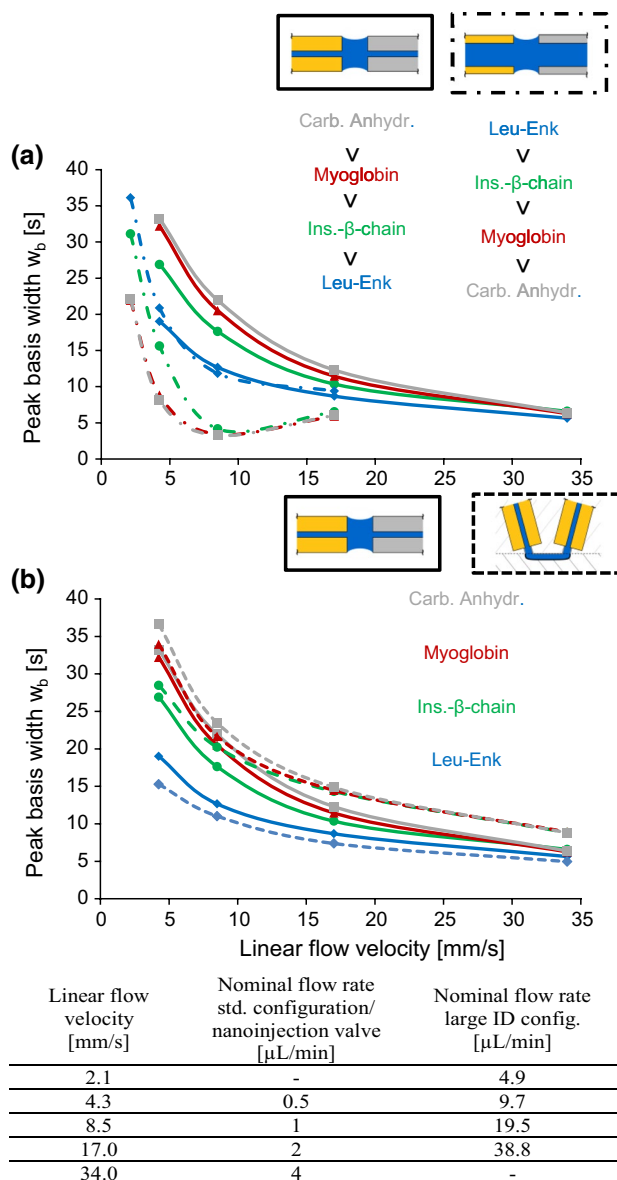
creeping flow and transport of diluted species modules. No slip was assumed for the solid–liquid interfaces, while full slip was assumed for the air–liquid interfaces. The flush-out profiles were calculated at the outlet of the ESI spray tip.

The geometry of the simulated liquid gap was taken from the experimental setup: The liquid gap was 200 µm long,

Linear flow velocity [mm/s]	Nominal flow rate std. configuration/ nanoinjection valve [µL/min]	Nominal flow rate large ID config. [µL/min]
2.1	-	4.9
4.3	0.5	9.7
8.5	1	19.5
17.0	2	38.8
34.0	4	-

Fig. 1 Analysis of peak basis widths after 10-nL sample injection by using two different capillary configurations (**a**) and a nano-injection valve (**b**). *Plotted* are averaged peak basis widths w_b in dependence of the linear flow velocity of the system buffer. The sample comprises four analytes with distinct differences in molecular weight: leucine-enkephalin (Leu-Enk): 555 Da; insulin-β-chain: ~3.5 kDa; myoglobin: ~17.0 kDa; carbonic anhydrase: ~29.1 kDa; sample solvent: H_2O; system buffer: H_2O/MeOH, 50:50, 0.1 % FA; pos. ESI-MS detection. Peak widths were determined by using extracted ion chromatograms of the most abundant ion species each and averaging over five technical replicates (see also Table 2)

Table 2 Parameters and statistics of the injection series shown in Fig. 1

	Leu-Enk	Insulin β-chain	Myoglobin apoenzyme	Carbonic anhydr.
Analyte characteristics				
Most abundant ion species	$[M + H]^+$	$[M + H]^{3+}$	$[M + H]^{21+}$	$[M + H]^{31+}$
Molecular weight (Da)	556	3.5 k	17 k	29 k
Extracted mass range (Da)	556.3 ± 0.15	1166.3 ± 0.15	808.3 ± 0.5	937.3 ± 0.5
Analyte conc. (µM)				
Std. config./Inj. valve	18	50	12	24
Large ID config.	90	250	66	128
Abs. amount injected (ng); $V_{inj} = 10\ nL$				
Std. config./Inj. valve	0.1	1.7	2.0	7.0
Large ID config.	0.5	8.7	11.2	37.3
Averaged SD in w_b of technical replicates (s)				
Std. config.	0.4	0.4	0.8	0.8
Large ID config.	0.5	0.7	0.7	0.7
Inj. valve	0.3	0.6	0.7	0.6
Averaged rel. SD in peak area of technical replicates (%)				
Std. config.	12	14	17	18
Large ID config.	9	14	11	10
Inj. valve	5	6	11	10

while the capillaries had an outer diameter of 360 µm and an inner diameter of 220 (large ID configuration) and 50 µm (standard configuration), respectively. The equilibrium waist diameter of the liquid bridge was set 260 µm, as observed in the experiments (Neu et al. 2013). The downstream ESI spray tip was simulated over its full 50 mm length.

The physical properties of the liquid were derived from the used buffer at 25 °C (density 930 kg/m³ viscosity 0.016 Pa s). The linear flow velocity was set to 8.5 mm/s, reproducing the most common experimental condition of the measured molecules Leu-Enk and myoglobin.

The diffusion coefficient of Leu-Enk in water is reported to be 4×10^{-10} m²/s (Gerhardt and Adams 1982). Taking into account that the diffusion coefficient is inversely proportional to the medium viscosity, we estimated a diffusion of 2.5×10^{-10} m²/s for LEU-ENK in our buffer. Myoglobin typically has a diffusion coefficient of 1×10^{-10} m²/s in water (Riveros-Moreno and Wittenberg 1972); however, it denatures in the buffer used, which yields a ~4 smaller diffusion coefficient (Choi and Terazima 2002). Taking again into account the viscosity of the used buffer, we estimated a diffusion coefficient of 1.6×10^{-11} m²/s for myoglobin.

3 Results and discussion

3.1 Experimental studies with ESI-MS detection

For the analysis of nanoliter sample infusion into an open liquid bridge, we compared two different capillary configurations using a capillary gap sampler. A commercial nanoliter injection valve was used as a benchmark. Configuration details of these systems are listed in Table 1.

In order to systematically investigate the relevant microfluidic and physical parameters that govern sample flush-out, a set of four analytes was selected, which cover a broad mass range (0.5–29 kDa). Injections were performed under denaturing conditions, such that analyte characteristics related to protein folding are suppressed, and large differences of the diffusion coefficients can be expected. The experimental part of the study mainly comprised the analysis of the peak base width w_b as a function of the linear flow velocity, which allows for a uniform comparison of different system configurations (see Fig. 1). Moreover, the temporal base width of the signals, w_b, as a measure for the flush-out was selected because (1) it was found to be much less dependent from analyte concentration compared to analyte peak area over a broad range of almost two orders of magnitude (see Fig S2, Tab. S1 in the supplementary information), and (2) because it is directly related to the sample throughput of a flow injection system. Figure 1a shows the analyte peak width at four different linear flow velocities for the standard capillary configuration (solid lines), with different analytes being encoded by different colors. As one may expect, the sharpest peaks with the smallest w_b are observed at the highest linear flow velocity. Moreover, differences in w_b continuously decreased with the linear flow velocity, i.e., the influence of molecular diffusion is reduced at high flow rates.

The order of the solid curves clearly follows the analyte molecular weight (MW) from large to small, which implies that diffusion coefficients of the analytes play a crucial role

for the sample flush-out process. We attribute this relationship between the diffusion coefficients and the peak width to dead zones at the capillary entry, which act as diffusion limited traps for the molecules, and to dispersion within the capillary due to lateral diffusion. More details can be found in Sect. 3.2 together with numerical simulations.

We could exclude longitudinal diffusion along the capillary as dominant factor, due to the short capillary length and the high flow velocity. Absorption at the capillary wall has a negligible influence because of the short dwell time and the little surface area and is not considered either for our explanations.

3.1.1 Thin capillary wall inverts the dependence of peak width on MW

By comparing the dashed curves with the solid curves shown in Fig. 1a, it is obvious that the capillary wall thickness plays a major role in sample flush-out behavior. Moreover, the analyte MW determines how distinct the differences are. For a small molecule like Leu-Enk, the curves for both capillary configurations shown in Fig. 1a nearly overlap. In contrast, for the larger molecules, peak widths decrease by up to a factor of 4 when the large ID capillary configuration is used. In other words, the relationship w_b versus MW is inverted when changing from the standard capillary configuration to the large ID configuration. Moreover, in case of the large ID configuration, a clear minimum in w_b can be observed for the larger molecules at a linear flow velocity of 8.5 mm/s. The curves also suggest that there are different "hot spots" in parameter space for an optimal sampler performance, depending on the capillary geometry and the linear flow velocity. Nevertheless, when setting the buffer flow rate, one should also keep in mind that there are limitations on system backpressure and effects on electrospray performance (see corresponding Sect. 2, and Fig. S3 in the supplementary information).

The optimum flow speed of 8.5 mm/s which is observed in Fig. 1a for the large ID case and large molecules, we attribute to a "repelling" effect of faster stream velocities against the injected volume. That prevents the analyte from fully entering the stream, which in turn confines the majority of molecules closer to the capillary wall, resulting in a broader peak. For the smallest molecule Leu-Enk, the effect is less pronounced, because of the high diffusion coefficient. That leads to stronger mixing in the channel, allowing more molecules to reach the fast streamlines in the capillary center. Corresponding simulations are mentioned in Sect. 3.2.4.

3.1.2 Comparison with nano-injection valve

The comparison of the standard capillary configuration with the nano-injection valve in Fig. 1b reveals quite

similar sample flush-out behavior. Again, the smallest molecule is less influenced by the change in system configuration, which results in close and nearly parallel curve courses. Also the curves of the larger molecules overlap for both configurations at lowest linear flow velocity, before they run into different minima in w_b toward highest linear flow velocity. Presumably, the presence of similar dead zones in both configurations is the main reason for the similarity in the curves. In case of the standard capillary configuration, dead zones are located within the gap close to the capillary walls. For the nano-injection valve several dead zones exist at the transition from rotor (about 150 μm I.D.) to stator bores (100 μm I.D.) to the capillaries (50 μm I.D.) and in the corners opposite the stator bores due to the change in flow direction.

3.1.3 Injection parameters and statistics

Parameters and statistics of the injection series data are summarized in Table 2. In comparison with the standard configuration of the capillary gap and the nano-injection valve, an at least fivefold higher sample concentration has been injected when using the large ID configuration. This was due to the expectation of a lower efficiency in electrospray ionization for the large ID configuration, based on (1) a larger capillary ID, (2) an almost tenfold higher volumetric flow rate in the absence of supporting gases at the electrospray interface, and (3) the use of a non-tapered spray nozzle (see also Fig. S3). An averaged SD in w_b of <1 s for each system configuration underlines the suitability of the parameter w_b as a marker for system characterization. The analysis of relative SD in peak area shows an expected trend: sample uptake using a solid pin causes a higher deviation in sample volumes injected (9–18 %) compared to a nano-injection valve (5–11 %).

3.1.4 Comparing the flush-out of myoglobin and leucine-enkephalin

In addition to peak base widths, corresponding peak profiles can also give valuable insights into the sample flush-out process. In this context, Fig. 2 shows overlaid peak profiles of leucine-enkephalin as the smallest analyte (blue) and of myoglobin (red) with a ca. 30-fold higher MW. Moreover, pairs of peak profiles are shown in different rows for the different system configurations, and different in columns for the different linear flow velocities.

For a better overview, only peak profiles at identical linear flow velocities are shown. The most striking difference in peak profile appears for the large ID capillary configuration compared to the other two system configurations. In the latter cases, the rising edge of the myoglobin peak is always in front to that of Leu-Enk. Moreover,
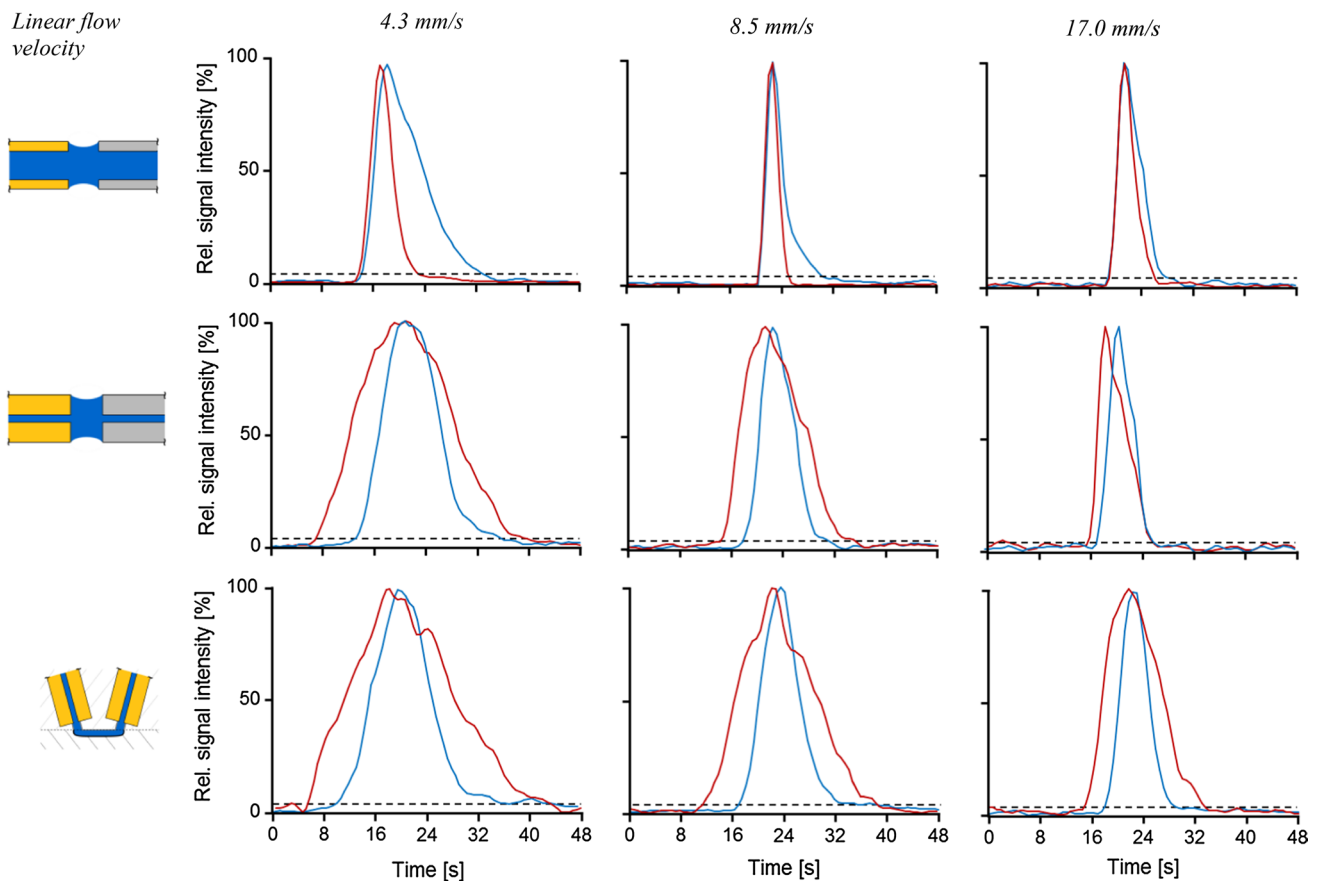
Fig. 2 Comparison of sample flush-out profiles after 10 nL sample infusion. Compared are representative sample flush-out profiles of leucine-enkephalin (*blue*) and myoglobin (*red*) at three different linear flow velocities, by using two different capillary configurations and a commercial nano-injection valve. Profiles are generated by using extracted ion chromatograms of the $[M + H]^+$ ion of Leu-Enk at m/z = 556.3 ± 0.15 Da and the $[M + H]^{21+}$ ion of myoglobin at m/z = 808.3 ± 0.50 Da, and by performing minor data smoothing. The *dashed line* marks the threshold for determination of peak basis width in Fig. 1, which has been set at 5 % relative peak height

the peaks are quite symmetric, which leads to an "enclosure" of the peak profile of Leu-Enk by that of myoglobin, except in the standard capillary configuration at highest linear flow velocity. In contrast, for the large ID capillary configuration, the peak profiles show a quite steep and nearly identical rising edge, such that differences in peak profiles are mainly due to differences in the tailing parts of the peaks. Another characteristic concerns a small but persistent "peak smearing," which is indicated by an offset in extracted ion chromatograms EIC base lines before and after each peak, and most pronounced at lower linear flow velocities. Reasons could be due to (1) the geometry of compartments and the presence of "dead zones," which are less efficiently flushed out by the buffer stream, and (2) a lowered efficiency in electrospray at higher linear flow velocities, which causes a restricted detection of signals close to the spectral noise. In this context, the OD/ID ratio of capillaries forming the gap is supposed to play a major role. A change in ratio from 7.2 to 1.8 for the large ID capillary configuration should cause both a more efficient sample flush and a comparably low efficiency in electrospray.

3.2 Simulations reproduce and explain the main characteristics of the measurements

For the simulations we used the simplest possible boundary and initial conditions which could still reproduce the main characteristics of the measured results. The assumption of complete mixing of the sample in the gap, just after injection, was found to represent the experiments well enough.

The results are shown in Figs. 3, 4, 5, 6 and 7. Figure 3 shows the standard case; the experimental base width and the leading edge of the myoglobin peak are reproduced well by the simulation. However, an initial spike of myoglobin is present in the simulation, which was not observed in the experiments, probably due to the simplified initial conditions. Figure 4 shows the large ID configuration, where both Leu-Enk and myoglobin reach the MS simultaneously, as observed experimentally. The generally broader peak of
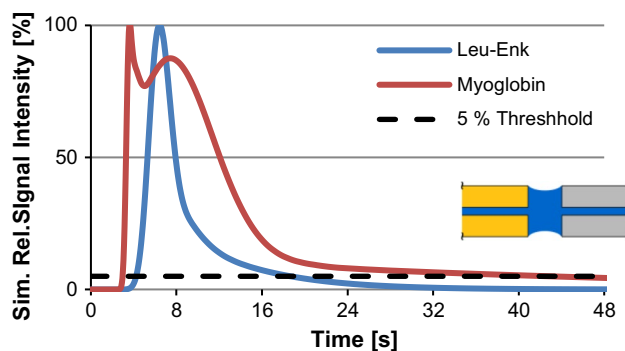
Fig. 3 Simulated flush-out profile of the standard configuration. As in the measured flush-out profile of Fig. 2, myoglobin reaches the outlet first, yet has a much wider peak than Leu-Enk. The steep flank of the myoglobin is a consequence of assuming a homogenously filled gap right after injection. The rising edge is less steep in reality, which indicates that the injection might not completely fill the gap. Another reason could be the reported time to equilibration, (Neu et al. 2013) within which the bridge goes from a "round belly" shape right after injection, to its equilibrium shape with a waist of 260 μm. During this time, the sample is slowly pushed toward the center of the capillary, taking the edge out of the flush-out profile. The *dashed line* marks the threshold for determination of peak basis width
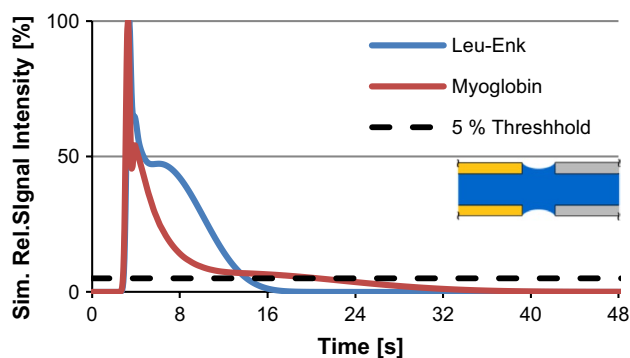

Fig. 4 Simulated flush-out profile of the large ID configuration. The simulations reproduce the main characteristics of the measured curves: myoglobin and Leu-Enk reach the outlet simultaneously. The peaks are generally thinner than for the standard configuration, and the myoglobin peak drops quickly compared to the Leu-Enk peak. The *dashed line* marks the threshold for determination of peak basis width

Leu-Enk compared to myoglobin is also nicely reproduced. There is, however, a tendency of the simulation to predict a longer peak base width than the experimentally measured w_b, and there is again an initial spike, probably due to the simple initial conditions. Figure 5 shows the simulated dispersion, which takes place within the ESI capillary. While there is no experimental data available for the peak shapes within the capillary, the simulated peak at the output is close in width and shape to its measured counterpart.

A better match between simulation and measurement is likely possible if the full dynamics of the injection process
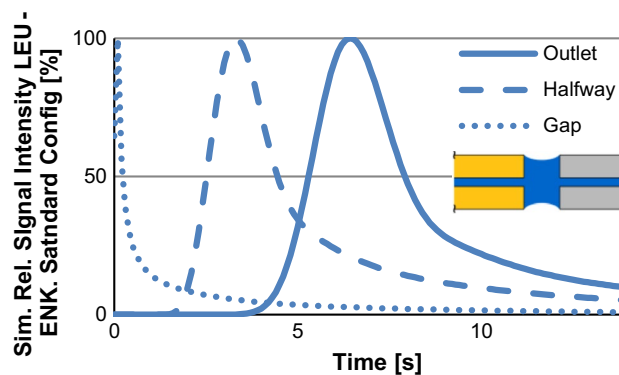

Fig. 5 Influence of dispersion in ESI capillary. The figure shows the simulated LEU-ENK peak over time at different positions of the ESI capillary in the standard configuration. Comparing the profile just after the gap, halfway into the capillary and at the outlet of the spray tip, the peak width (FWHM) increases from 0.3 to 2 s, and finally 2.6 s. The sample peak travels through the spray tip at almost constant speed; this can also be seen clearly in this figure. An analog peak broadening along the capillary is also observed for the large ID configuration (not shown)

are simulated, which is, however, beyond the scope of the present work. Specifically, this would include the time-dependent coalescence of the two liquid domains, and generating complex time- and geometry dependent gradient flows of the sample into the liquid gap.

3.2.1 Dead zones in the capillary gap explain broad myoglobin peak in the standard configuration

An important phenomenon in the capillary gap sampler are the dead zones within the gap where there is very little flow or even eddies which act as a laminar trap. Molecules with a high diffusion coefficient can leave these dead zones relatively quickly, while large, slowly diffusing molecules stay trapped for long times. The dead zones take up a major part of the gap volume of the standard configuration, but occupy much less space in the large ID configuration as shown in Fig. 6. 20 % of the injected myoglobin is still in the standard gap after 30 s, whereas less than 1 % remains in the gap in the large ID configuration after the same time; the corresponding simulation results are shown in Fig. 7. This explains the broader myoglobin flush-out profiles of the standard configuration compared to the large ID configuration. The dead zones get smaller with increasing flow speed, which is reflected in the fact that w_b generally gets thinner with increasing flow speed as seen in Fig. 2.

3.2.2 Dispersion in the ESI capillary explains why large molecules reach the outlet first

It is crucial to account for the sample dispersion within the ESI capillary to understand the observed flush-out profiles.
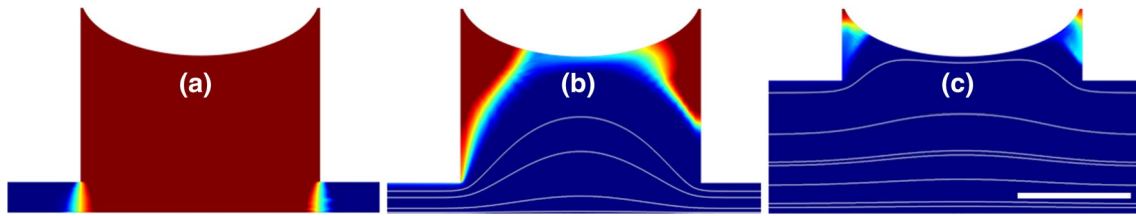
Fig. 6 Dead zones in the capillary gap. Shown is the relative concentration of injected material in the gap for myoglobin. Visualized is a cut through the capillary gap; at the *bottom* is the axis of rotational symmetry; hence, only half the height is shown. The buffer flows from *right* to *left* with an average velocity of 8.5 mm/s. **a** the simple initial condition, where the gap is filled completely by the injected myoglobin (*red*). **b** Depicts the standard configuration after 8 s, with the streamlines shown in *white*, while **c** shows the large ID configuration after 8 s, again with the streamlines in *white*. The "dead zones" in the outer corners of the liquid bridge have almost zero convection; hence, it can capture a slowly diffusing molecule such as myoglobin. The large ID configuration exhibits much smaller "dead zones" for obvious geometrical reasons. The *scale bar* in **c** corresponds to 100 μm
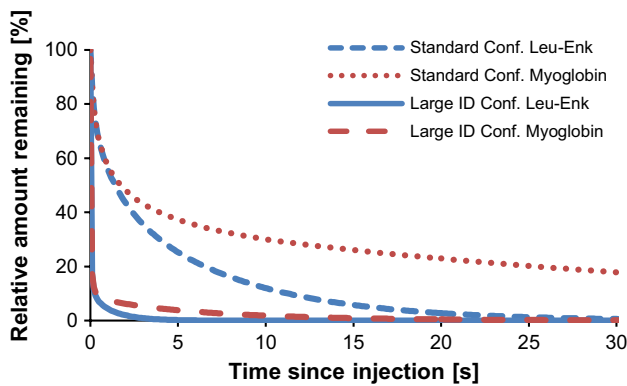

Fig. 7 Remaining material in the dead zones of capillary gap. Shown is the relative amount of injected material remaining in the gap. It is much more for the standard configuration where 20 % of the myoglobin is still captured by "dead zones" even 30 s after the injection

Typically this phenomenon is described by the Taylor–Aris dispersion (TAD) (Aris 1956). However, simple TAD models apply only if the molecules travel along the capillary for much more time than they need to diffuse across the capillary cross-section (Wissler 1969). This is not the case for our setup (as seen in Table S2). For this reason, the ESI channel was integrated along its full length into the simulations and the effective dispersion was found numerically with COMSOL.

Dispersion effects explain why large molecules reach the outlet before small molecules, as can be observed in Figs. 2 and 3: the laminar velocity profile in the capillary has its maximum in the center of the capillary and its minimum at the capillary wall. A very small molecule with a very large diffusion will travel through all speed zones. Thus at the end of the capillary, it will appear as if the molecule has travelled with the average velocity of the laminar flow (see Fig. 5 for the effect on LEU-ENK). An extremely large molecule will, however, have no diffusion. Therefore, it will stay within the same speed zone until it reaches the outlet. So, if myoglobin (large molecule) started to flow through the capillary in a "high speed zone," close to the center of the capillary, it will reach the outlet very fast, while it will almost not move for long times if it starts moving through the capillary close to the capillary wall. This supports the assumption of a sample injection that spreads evenly in the gap. Thus, a significant amount of molecules start in the fast, central region of the capillary flow. They can therefore reach the outlet before smaller molecules, which tend to diffuse into regions of slow flow close to the wall. Dispersion is also the reason why the large ID configuration shows steeper rising edges in Fig. 2, while the standard configuration has more symmetric peaks (as seen in Fig. 5). A larger inner diameter increases the time a molecule needs to diffuse across the capillary cross-section, therefore increasing the time it stays within its initial speed zone. The result is a pronounced asymmetry in the flush-out profiles.

3.2.3 Dispersion and dead zones explain the inversion of w_b versus MW

Combining the effect of the dispersion with the dead zones the "w_b versus MW" inversion encountered in Fig. 2 is reproduced by the simulations in Figs. 3 and 4. The dispersion lets large molecules generally reach the outlet first, yet the dead zones in the standard configuration keep large molecules trapped. In effect, the myoglobin engulfs the flush-out peak of the smaller Leu-Enk. In contrast, there are almost no dead zones in the large ID configuration, and all molecules leave the gap quickly as seen in Fig. 7. They are then only influenced by dispersion, which results in a clearly reduced peak width for myoglobin.

3.2.4 Repelling of injection leads to broader peaks

As can be observed in Fig. 1a, the optimal flow speed for the large ID configuration was found at 8.5 mm/s. In

Sect. 3.1.1, we attribute this to a repelling effect of the fast stream onto the injected volume. With simulations, we checked this hypothesis of a more shallow injection due to a repelling stream, where molecules would reach only 0.1 mm into the gap instead of the full radius (0.18 mm). Indeed for large, slow diffusing molecules, the simulated peaks would get broader for 17 mm/s flow speed than for 8.5 mm/s as observed in the measurements. For the small and fast diffusing Leu-Enk on the other hand, the higher flow speed still leads to narrower peaks. The corresponding plots are shown in the Supplementary information.

These simulations confirm that repelling will lead to broader peaks, especially for large molecules. The simulation, however, cannot tell the optimal flow speed depending of the capillary geometry. For that, the injection process itself would have to be simulated including how the injected volume touches the liquid bridge and merges with it. As mentioned in the beginning of Sect. 3.2 this was beyond the scope of this work, yet will likely be taken up in future publications.

3.2.5 Alternative initial condition could be rejected

Another possible, and very simple, initial condition was that the sample would first engulf the liquid bridge and then enter it by diffusion. However, if the injection would not reach into the gap, molecules would generally start at the capillary wall when entering the flow. This would broaden the flush-out profiles dramatically and lead to small molecules reaching the outlet first. This was not observed, and therefore, this alternative initial condition could be rejected. The influence of adsorption/desorption on the capillary wall and electroosmotic effects in the capillary gap were found to be negligible during the simulation and analysis of our measurements. Nevertheless, effects based on adsorption/desorption of analytes cannot be excluded when changing experimental conditions, such as the used sample solvents and buffers.

4 Conclusions

Measurements showed that the usage of a nano-injection valve and the standard capillary configuration leads to similar results with respect to sample flush-out characteristics, meaning that the peak width w_b decreases with the MW of analytes. This supports the assumption of a sample that mixes well within the gap during injection as an important boundary condition of the simulations. In contrast, the relationship between w_b and MW is inverted when changing to the large ID configuration due to significant peak tailing of small molecules. This inversion could be explained by finding the two driving factors behind the peak width for the

capillary gap sampler in simulations: (1) large molecules are being captured by dead zones in the capillary gap, and (2) small molecules are subject to significant dispersion in the ESI spray tip.

These insights give valuable guidelines for optimization of the ESI spray tip as interface between nanoliter sample infusion via a liquid bridge and electrospray ionization. The primary aims of the optimization are:

- *Minimized crosstalk between sample plugs* This implies short residence times of the sample in the capillary gap and a small peak width of the sample at the outlet. The result is an increased measurement quality and higher throughput.
- *Minimized internal volume of the spray tip* A lower volume implies a reduced buffer flow to reach the same buffer velocity and therefore a reduced dilution. Making the capillary shorter reduces the internal volume and also results in improved reaction times (the time until the first molecule of a sample plug reaches the mass spectrometer).
- *Enhanced efficiency in electrospray ionization* Optimized outlet geometry and gas support will affect the ESI ability to work with low sample amounts and concentrations.

This aims can be reached through miniaturization of the capillary gap and spray tip: As shown in this work, large sample molecules profit from a reduced wall thickness of the capillary because it results in much smaller "dead zones." A reduction in the length of the spray tip will decrease the residence time of sample plugs in the capillary and also reduce peak width based on less dispersion in the spray tip. A reduction in outer diameter of the capillary would also be beneficial because molecule diffusion as a limiting factor for flushing the capillary gap is faster over short distances. Additionally, the liquid bridge stability will increase (Neu et al. 2013). Finally, a reduction in the inner diameter reduces the internal volume of the spray tip and allows smaller volumetric flow rates to maintain appropriate linear flow velocities for more efficient electrospray ionization.

Reducing the capillary dimensions will also reduce the optimal distance between capillaries to form a liquid bridge. The solid pins for sampling will have to shrink accordingly to avoid wetting the outer surfaces of capillaries during injection. Consequently, the injected volumes could be reduced and lower concentrations will be expected at the outlet. A possibility to circumvent the problem could be the use of glass capillaries with a small outer diameter, yet large inner diameter, as active sampling devices.

With respect to the electrospray ionization efficiency, heated gas support and a reduced opening and wall

thickness of the spray nozzle compared to the standard capillary configuration would be beneficial in order to allow better analyte desolvation, a smaller initial droplet size, and higher electric field strength.

In conclusion, we recommend a very short (e.g., 10 mm) large ID spray tip, combined with a nozzle tapered to about 20 μm opening and a wall thickness as thin as possible, to give better sampler performance with respect to signal quality, throughput and electrospray efficiency. By implementing alternative sampling devices such as glass capillaries, the dimensions of the liquid bridge and spray tip could be further reduced, with positive impact on the characteristics of the setup.

References

Aris R (1956) On the dispersion of a solute in a fluid flowing through a tube. Proc R Soc Lond A 235:67–77. doi:10.1098/rspa.1956.0065

Choi J, Terazima M (2002) Denaturation of a protein monitored by diffusion coefficients: myoglobin. J Phys Chem B 106:6587–6593. doi:10.1021/jp0256802

Feng X, Liu X, Luo Q, Liu B-F (2008) Mass spectrometry in systems biology: an overview. Mass Spectrom Rev 27:635–660. doi:10.1002/mas.20182

Feng X, Liu B-F, Li J, Liu X (2014) Advances in coupling microfluidic chips to mass spectrometry. Mass Spectrom Rev 34:535–557. doi:10.1002/mas.21417

Gao D, Liu H, Jiang Y, Lin J-M (2013) Recent advances in microfluidics combined with mass spectrometry: technologies and applications. Lab Chip 13:3309–3322. doi:10.1039/c3lc50449b

Gasilova N, Yu Q, Qiao L, Girault HH (2014) On-chip spyhole mass spectrometry for droplet based microfluidics. Angew Chem Int Ed Engl 53:4408–4412. doi:10.1002/anie.201310795

Gerhardt G (2011) Microfluidics-based separations technology for the analytical laboratory. Chromatogr Today 4:6–8

Gerhardt G, Adams RN (1982) Determination of diffusion coefficients by flow injection analysis. Anal Chem 54:2618–2620. doi:10.1021/ac00251a054

Jian W, Romm MV, Edom RW, Miller VP, LaMarr WA, Weng N (2011) Evaluation of a high-throughput online solid phase extraction–tandem mass spectrometry system for in vivo bioanalytical studies. Anal Chem 83:8259–8266. doi:10.1021/ac202017c

Jin D-Q, Zhu Y, Fang Q (2014) Swan probe: a nanoliter-scale and high-throughput sampling interface for coupling electrospray ionization mass spectrometry with microfluidic droplet array and multiwell plate. Anal Chem 86:10796–10803. doi:10.1021/ac503014k

Koster S, Verpoorte E (2007) A decade of microfluidic analysis coupled with electrospray mass spectrometry: an overview. Lab Chip 7:1394–1412. doi:10.1039/B709706A

Mayr LM, Bojanic D (2009) Novel trends in high-throughput screening. Curr Opin Pharmacol 9:580–588. doi:10.1016/j.coph.2009.08.004

Neu V, Steiner R, Müller S, Fattinger C, Zenobi R (2013) Development and characterization of a capillary gap sampler as new microfluidic device for fast and direct analysis of low sample amounts by ESI-MS. Anal Chem 85:4628–4635. doi:10.1021/ac400186t

Nge PN, Rogers CI, Woolley AT (2013) Advances in microfluidic materials, functions, integration, and applications. Chem Rev 113:2550–2583. doi:10.1021/cr300337x

O'Brien JT, Williams ER, Holman H-YN (2015) Ambient infrared laser ablation mass spectrometry (AIRLAB-MS) of live plant tissue with plume capture by continuous flow solvent probe. Anal Chem 87:2631–2638. doi:10.1021/ac503383p

Oh KW, Ahn CH (2006) A review of microvalves. J Micromech Microeng 16:R13–R39. doi:10.1088/0960-1317/16/5/R01

Ohla S, Belder D (2012) Chip-based separation devices coupled to mass spectrometry. Curr Opin Chem Biol 16:453–459. doi:10.1016/j.cbpa.2012.05.180

Ovchinnikova OS, Kertesz V, Van Berkel GJ (2011) Combining laser ablation/liquid phase collection surface sampling and high-performance liquid chromatography—electrospray ionization-mass spectrometry. Anal Chem 83:1874–1878. doi:10.1021/ac200051y

Park S-G, Murray KK (2012) Infrared laser ablation sample transfer for on-line liquid chromatography electrospray ionization mass spectrometry. J Mass Spectrom 47:1322–1326. doi:10.1002/jms.3096

Pei J, Li Q, Kennedy RT (2010) Rapid and label-free screening of enzyme inhibitors using segmented flow electrospray ionization mass spectrometry. J Am Soc Mass Spectrom 21:1107–1113. doi:10.1016/j.jasms.2010.02.013

Riveros-Moreno V, Wittenberg JB (1972) The self-diffusion coefficients of myoglobin and hemoglobin in concentrated solutions. J Biol Chem 47:895–901

Roach PJ, Laskin J, Laskin A (2010) Nanospray desorption electrospray ionization: an ambient method for liquid-extraction surface sampling in mass spectrometry. Analyst 135:2233–2236. doi:10.1039/c0an00312c

Růžička J (1992) The second coming of flow-injection analysis. Anal Chim Acta 261:3–10. doi:10.1016/0003-2670(92)80169-8

Sun S, Slaney TR, Kennedy RT (2012) Label free screening of enzyme inhibitors at femtomole scale using segmented flow electrospray ionization mass spectrometry. Anal Chem 84:5794–5800. doi:10.1021/ac3011389

Van Berkel GJ, Kertesz V (2015) An open port sampling interface for liquid introduction atmospheric pressure ionization mass spectrometry. Rapid Commun Mass Spectrom 29:1749–1756. doi:10.1002/rcm.7274

Van Berkel GJ, Kertesz V, King RC (2009) High-throughput mode liquid microjunction surface sampling probe. Anal Chem 81:7096–7101. doi:10.1021/ac901098d

Volný M, Rolfs J, Hakimi B, Fryčák P, Schneider T, Liu D, Yen G, Chiu DT, Tureček F (2014) Nanoliter segmented-flow sampling mass spectrometry with online compartmentalization. Anal Chem 86:3647–3652. doi:10.1021/ac500365r

Wissler EH (1969) On the applicability of the Taylor–Aris axial diffusion model to tubular reactor calculations. Chem Eng Sci 24:527–539. doi:10.1016/0009-2509(69)85024-4

Yin H, Killeen K, Brennen R, Sobek D, Werlich M, van de Goor T (2005) Microfluidic chip for peptide analysis with an integrated HPLC column, sample enrichment column, and nanoelectrospray tip. Anal Chem 77:527–533. doi:10.1021/ac049068d